Int. J. Solids Structures, 1965, Vol. 1, pp. 97 to 111. Pergamon Press Ltd. Printed in Great Britain

PLASTIC BEHAVIOR OF SIMPLY SUPPORTED REINFORCED CONCRETE PLATES AT MODERATELY LARGE DEFLECTIONS

ANTONI SAWCZUK*

Polish Academy of Sciences, Warsaw

and

LECH WINNICKI

Warsaw Polytechnic Institute, Warsaw

Abstract—It is known from experiments that the actual load-carrying capacities of plates are larger than those predicted by the limit analysis theory. The behavior of plastic structures beyond the bending collapse load is influenced by the changes in geometry of a structure during the process of plastic deformation. In the present paper, an investigation of the load–deflection relationship for simply supported rectangular reinforced concrete plates is presented. The tensile membrane action is found to be localized in zones of bending yield hinges. The zones of pure membrane response consequently develop as the load increases. The paper presents a kinematical method of analysis of plastic plates beyond the bending collapse load. Kinematically admissible collapse modes are studied and the associated dissipation functions are derived. Load–deflection relationships are obtained for various yield patterns. The theoretical results are compared with experimental data following from model tests.

1. INTRODUCTION

TWO MAIN factors influence the behavior of plastic structures beyond the plastic collapse load, namely the material strain-hardening and the changes in geometry of a structure during the process of plastic deformation. For the purpose of structural design of reinforced concrete plates the influence of hardening on the ultimate load is easy to estimate, simply by substituting the actual ultimate strength instead of the yield stress of reinforcing bars. From experiments on the plastic behavior of transversely loaded reinforced concrete plates it follows that deflection at the state of instability of the deformation process cannot be considered small. It is also observed that the actual load carrying capacities of plates are higher than those predicted by the limit analysis theory (even with the appropriate modifications for the hardening effects). Therefore an investigation is required which would take into account the changes in geometry of a structure in the process of plastic deformation.

The importance of the problem of post-yield behavior of reinforced concrete plates has already been pointed out by Gvozdev [1]. However, only recently a satisfactory analysis concerning circular plates has been presented by Wood [2]. The methods of plastic analysis, of rotationally symmetric, perfectly plastic shells have provided some hints for derivation of load–displacement relations for circular plates (see [3–5]). A rectangular plate problem cannot, unfortunately, be approached in the same way, since a prerequisite for it is the complete limit analysis solution for bending. This, however, cannot be obtained, except for very particular cases of loading. Therefore methods of appropriate bounding of the load–deflection relation beyond the yield point load are needed, (see [6, 7]).

* Present address: Department of Mechanics, Illinois Institute of Technology, Chicago, Illinois 60616, U.S.A.

It follows from experiments on rectangular plates that either the post-yield membrane action in reinforced concrete plates is localized in zones of bending yield hinges, or certain additional 'membrane hinges' appear. This fact seems to have been noticed for the first time by Wood [2]. The experiments by Jaeger, [8], Sawczuk *et al.*, [9], rendered some evidence in this respect.

In the present paper an investigation of the load–deflection relationship for simply supported rectangular plates is presented. Both theoretical and experimental results are given. To make the paper self-contained, in Section 2 basic relations of the plastic theory of plates at moderately large deflections are recalled. The curves of bending-axial forces interaction for reinforced concrete sections are briefly discussed in Section 3. Kinematically admissible collapse modes and the associated dissipation functions are analyzed in Section 4, whereas Section 5 presents the load–deflection relations following from the developed approximate theory. Section 6 contains a description of the test arrangements and models. Recorded and theoretical load–deflection relations are compared in Section 7, the yield patterns being also given.

2. BASIC RELATIONS

In the present analysis, if not stated otherwise, the rigid-perfectly plastic model of deformation is employed. Thus, in the deforming zones an appropriate yield condition has to be fulfilled. For plates subjected to bending, the yield condition $F = \text{const.}$ is expressed in terms of the stress couples tensor $M_{\alpha\beta}$, $(\alpha, \beta = 1, 2)$, namely $F(M_{\alpha\beta}) = \text{const.}$ At increasing deflections of a plate the membrane forces $N_{\alpha\beta}$ appear, therefore the yield condition takes the form $F(M_{\alpha\beta}, N_{\alpha\beta}) = \text{const.}$ Since components of the $N_{\alpha\beta}$-tensor are deflection dependent, so is the stress profile on the yield hypersurface F.

The plastic deformation is accompanied by internal energy dissipation. In the presence of bending and stretching, the dissipation density per unit area of the undeformed plate middle plane takes the form

$$d = M_{\alpha\beta}\dot{\kappa}_{\alpha\beta} + N_{\alpha\beta}\dot{\lambda}_{\alpha\beta}, \tag{1}$$

where $\dot{\kappa}_{\alpha\beta}$ stands for the curvature rates, $\dot{\lambda}_{\alpha\beta}$ being the components of the extension rates of the middle surface. If the plastic deformation process is to continue, the rate at which the external forces do work must not be smaller than the rate of internal work. For a plate of area A, this leads to the relation

$$\int_A p\,\dot{W}\,\mathrm{d}A \geq \int_A d\,.\,\mathrm{d}A = \int_A (M_{\alpha\beta}\dot{\kappa}_{\alpha\beta} + N_{\alpha\beta}\dot{\lambda}_{\alpha\beta})\,\mathrm{d}A, \tag{2}$$

where p stands for the transverse loading and $\dot{W}$ is the deflection rate. Since $M_{\alpha\beta}$, $N_{\alpha\beta}$ appearing in (2) are interconnected, in the process of plastic flow, by a deflection-dependent relation $F(M_{\alpha\beta}, N_{\alpha\beta}) = \text{const.}$, therefore (2) represents an estimation of the load–deflection relationship for plates at large deflections. If the plastically deforming regions can be localized at n generalized hinges, then the relation (3) takes the following form (cf. [7])

$$\int_A p\,\dot{W}\,\mathrm{d}A \geq \sum_1^n (N\dot{\Lambda}_i + M\dot{\theta}_i)l_i, \tag{3}$$

where $\dot{\Lambda}_i$ and $\dot{\theta}_i$ stand for the concentrated elongation and rotation of the plate median

surface at the ith generalized hinge, l_i is the length of the respective hinge line, M and N being respectively the bending moment and the axial force normal to the hinge line.

Let W denote a current, finite deflection at the yield hinge. If the distance between the yield hinge and the rotation axis is c, then from geometry of deformation (cf. [10]) it follows that

$$\theta = W/c, \qquad \Lambda = W^2/2c. \tag{4}$$

The appropriate rates of deformation entering the relation (3) are

$$\dot{\theta} = \dot{W}/c, \qquad \dot{\Lambda} = W\dot{W}/c = W\dot{\theta}. \tag{5}$$

Substitution of (5) into (3) yields the result

$$\int_A p\,\dot{W}\,\mathrm{d}A \geq \sum_1^n (NW + M)\dot{\theta}_i l_i, \tag{6}$$

which involves the actual deflection W of the hinge line.

For polygonal plates, $\dot{W}$ at any hinge line is expressible in terms of the rotation rates $\dot{\theta}_i$; thus the rate variables can be eliminated from (6) and an estimation of the load–deflection relationship can be obtained. This involves only the M and N stress resultants at the hinge, therefore the resultants normal to the hinge line. No other stress resultants contribute to the internal energy dissipation, therefore such a particular projection of the yield surface $F(N_{\alpha\beta}, M_{\alpha\beta}) = 0$ is required which involves the stress resultants M and N only.

3. PLASTIC INTERACTION CURVES

For a thinwalled spatial reinforced concrete structure the yield condition is an intersection of two hypercylinders $F_1(N_1, M_1) = 0$ and $F_2(N_2, M_2) = 0$ in the space of principal stress resultants N_1, N_2, M_1, M_2, (cf. [11], [12]). Since the subspaces N_1, M_1 and N_2, M_2 are orthogonal, the projection of the yield surface to the N_1, M_1 space is geometrically the same as an intersection of the yield surface by the planes $M_2 = N_2 = \text{const}$. This allows us to consider only the yield interaction curve of resultants $M_1 = M$ and $N_1 = N$. In this way the problem of yield condition is reduced to evaluation of an interaction curve in the M–N-plane.

Let us consider a cross section of unit width, reinforced at a distance H from the plate middle plane. The plate thickness is $2H$ and F_z denotes the reinforcement area per unit length and normal to the cross section. The geometry of deformation at the yielding cross section and the associate stress distribution at the state of failure are shown in Fig. 1(a) and 1(b) respectively.

If the axis of rotation of the collapse mechanism link lies in the undeformed plate middle plane then from the analysis of geometry of deformation the following relation is obtained

$$\zeta H = \Lambda/\theta = W/2, \tag{7}$$

where W denotes the actual deflection at the generalized hinge.

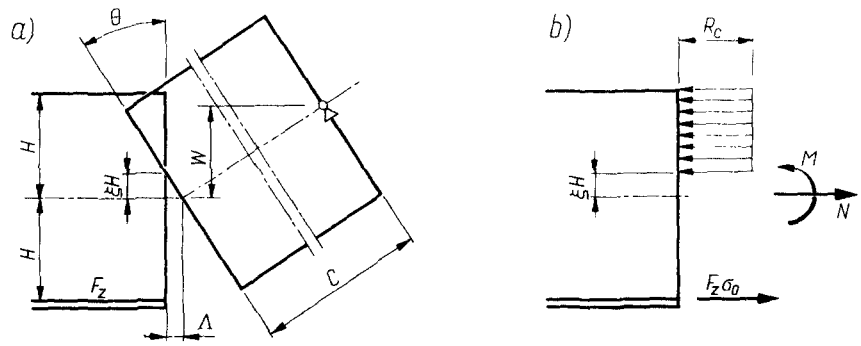

FIG. 1

On the other hand, the equilibrium requirements supply the expressions for the resulting normal force N and the bending moment M. In dimensionless form the respective expressions are

$$n = \frac{N}{N_0} = \begin{cases} 1 - \dfrac{1-\xi}{1-\xi_0}, & \xi_0 \le \xi \le 1, \quad (8) \\ 1, & \xi \ge 1, \quad (9) \end{cases}$$

$$m = \frac{M}{M_0} = \begin{cases} \dfrac{1}{3+\xi_0}\left(2 + \dfrac{1-\xi^2}{1-\xi_0}\right), & \xi_0 \le \xi \le 1, \quad (10) \\ \dfrac{2}{3+\xi_0}, & \xi \ge 1, \quad (11) \end{cases}$$

where

$$N_0 = F_x\sigma_0 = R_cH(1-\xi_0), \qquad 2M_0 = R_cH^2(1-\xi_0)(3+\xi_0), \tag{12}$$

stand for the ultimate tensile force and the ultimate moment at the cross section, respectively. The parameter ξ_0 appearing in the above relations denotes the neutral layer distance at the state of stress such that $N = 0$ and $M = M_0$, i.e. at the bending collapse. The magnitude of ξ_0 depends on the percentage of reinforcement and the properties of materials employed

$$\xi_0 = 1 - F_z\sigma_0/HR_c, \tag{13}$$

namely upon the concrete compressive strength R_c and the yield stress σ_0.

In view of (13) it can be concluded that the membrane action in reinforced concrete plates appears at a specified deflection of the yield hinge. The minimum deflection for the membrane action to develop is $W_{\min} = 2H\xi_0$.

By appropriate combination of the relations (7)–(11), the stress resultants in terms of deflections can be obtained and therefore the load deflection relation (3) can be evaluated for an actually considered collapse mode.

Elimination of ξ from the relations given above yields the interaction curve

$$m + 2n\frac{\xi_0}{3+\xi_0} + n^2\frac{1-\xi_0}{3+\xi_0} - 1 = 0, \tag{14}$$

which depends upon ξ_0, i.e. upon the percentage of reinforcement. Evaluation of the

load–deflection relation may be facilitated if the interaction curve (14) is properly approximated. For $0 \leq n \leq 1$, which is the case in the membrane action of plates, the interaction curve can be linearized to the form

$$m+n\frac{1+\xi_0}{3+\xi_0}-1=0. \tag{15}$$

Under such approximation the stress resultants take the following deflection-dependent form

$$n=\begin{cases}\dfrac{\dfrac{W}{2H}-\xi_0}{1-\xi_0}, & \xi_0 \leq \xi \leq 1, \quad (16)\\ 1, & \xi \geq 1, \quad (17)\end{cases}$$

$$m=\begin{cases}\dfrac{3-\xi_0-\dfrac{W}{2H}(1+\xi_0)}{(3+\xi_0)(1-\xi_0)}, & \xi_0 \leq \xi \leq 1, \quad (18)\\ \dfrac{2}{3+\xi_0}, & \xi \geq 1. \quad (19)\end{cases}$$

In the range of $0 \leq n \leq 1$ and $1 \leq m \leq 2/(3+\xi_0)$ the respective interaction curves are shown in Fig. 2. For $0 \leq \xi_0 < 1$ all interaction curves lie within the bounds traced in this figure by the lines AB_0 and AB_1.

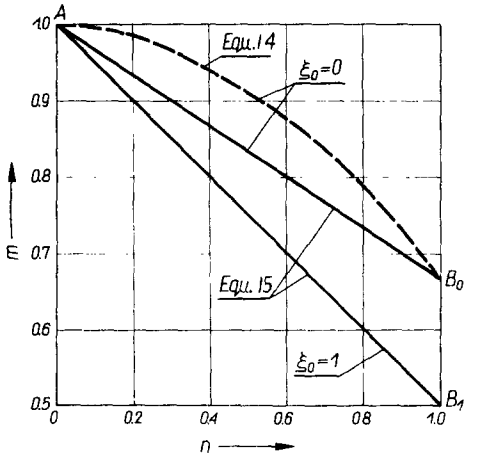

FIG. 2

If equation (12) is substituted into the expressions for the internal dissipation, the following relation for the dissipation function per unit length of the hinge is obtained:

$$d_i=(NW+M)\dot{\theta}_i=M_0\left(m+\frac{2n}{3+\xi_0}\frac{W}{H}\right)\dot{\theta}_i. \tag{20}$$

For the yield curve as given by equations (16)–(19) the dissipation function takes the deflection-dependent form

$$d_i = \begin{cases} \left[1+\dfrac{4\delta-1-\xi_0}{(3+\xi_0)(1-\xi_0)}(\delta-\xi_0)\right]M_0\dot{\theta}_i, & \xi_0 \le \xi \le 1, \qquad (21) \\ \dfrac{2}{3+\xi_0}(1+2\delta)M_0\dot{\theta}_i, & \xi \ge 1, \qquad (22) \end{cases}$$

where $\delta = W/2H$ denotes a dimensionless deflection.

For a particular collapse mode the internal dissipation can be computed. It is seen from (21) that the load–deflection relationship is non-linear. To evaluate the p–δ dependence, it is necessary to study the possible collapse modes of reinforced concrete plates.

4. COLLAPSE MODES

It can be learned from experiments on rectangular reinforced concrete plates that at early stages of the post-yield behavior, therefore for moderately large deflections, the yield pattern does not change but remains that of the bending response. Therefore the membrane action can be 'localized' at the yield hinges.

For a plate with edges restrained against sliding but free to rotate, a kinematically admissible collapse mode is shown in Fig. 3. Compressive forces equilibrating the membrane action are taken up by the supporting frame of the plate. In the case of symmetry the collapse mode is defined by a single parameter η, to be evaluated according to the yield line theory (cf. [13], [14])

$$\eta = \frac{1}{2\alpha^2}[\sqrt{(1+3\alpha^2)}-1], \qquad \alpha = \frac{a}{b}. \qquad (23)$$

At deflections $W = 2\xi_0 H$ the membrane forces begin to dissipate energy. Along the yield hinges shown in Fig. 3 three zones have to be distinguished. Within the range of deflections $0 \le W \le 2\xi_0 H$, defined by the parameters ψ_0 and β_0, only bending moments do work. Along the line KL there is $2\xi_0 \le W \le 2H$, therefore the dissipation has to be computed according to equation (21). For $W \ge 2H$ the expression (22) holds.

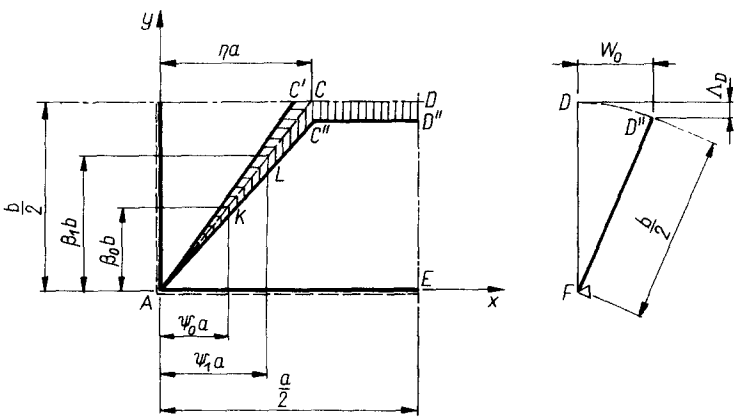

FIG. 3

If W_0 denotes the maximum deflection of the line CD, then

$$\beta_0 = \frac{\xi_0 H}{W_0} = \frac{\xi_0}{2\delta_0}, \qquad \psi_0 = \eta\frac{\xi_0}{\delta_0}, \qquad \delta_0 \geq \xi_0, \tag{24}$$

$$\beta_1 = \frac{1}{2\delta_0}, \qquad \psi_1 = \eta\frac{1}{\delta_0}, \qquad \delta_0 \geq 1, \tag{25}$$

where $\delta_0 = W_0/2H$.

The internal energy dissipation is due to pure bending response within the range $0 \leq x \leq \psi_0 a$, combined bending-membrane response for $\psi_0 a \leq x \leq \psi_1 a$, and pure membrane action within the range $\psi_1 a \leq x \leq \eta a$. If we denote by D_0 the dissipation associated with the bending collapse, and by D the dissipation at the combined membrane-bending action, then for the considered collapse mode we have

$$D_0 = M_0\frac{a\dot{\theta}_{AE}}{2} + M_0\frac{b\dot{\theta}_{AB}}{2} = M_0\dot{W}_0\left(\alpha + \frac{1}{2\eta\alpha}\right). \tag{26}$$

The dissipation of combined response depends upon the magnitude of the maximum deflection and for $\xi_0 \leq \delta_0 \leq 1$ it becomes

$$D = M_0(\psi_0 a\dot{\theta}_{AE} + \beta_0 b\dot{\theta}_{AB}) + M_0\left(\dot{\theta}_{AE} + \dot{\theta}_{AB}\frac{b}{2\eta a}\right) \times$$

$$\times \int_{\psi_0 a}^{\eta a} \left[1 + \frac{4\delta - \xi_0 - 1}{(3+\xi_0)(1-\xi_0)}(\delta - \xi_0)\right] dx + M_0\dot{\theta}_{AE}\left(\frac{a}{2} - \eta a\right)\left[1 + \frac{4\delta_0 - \xi_0 - 1}{(3+\xi_0)(1-\xi_0)}(\delta - \xi_0)\right]$$

where $\delta = \delta_0 x/\eta a$, η and ψ_0 being defined by the relations (23) and (24), respectively. Integration yields the result

$$D = M_0 W_0 \left\{ \frac{1+4\eta^2\alpha^2}{2\eta\alpha} \left[\frac{(3-\xi_0) - \frac{\xi_0^2}{\delta_0}(3-\xi_0)\frac{1}{6} - \delta_0(5\xi_0+1)\frac{1}{2} + \frac{4}{3}\delta_0^2}{(3+\xi_0)(1-\xi_0)}\right] \right.$$

$$\left. + (\alpha - 2\eta\alpha)\left[\frac{(3-\xi_0) - \delta_0(5\xi_0+1) + 4\delta_0^2}{(3+\xi_0)(1-\xi_0)}\right]\right\} \tag{27}$$

By an analogous procedure the value of D for $\delta_0 > 1$ can be evaluated. Knowing the dissipation function, the load–deflection relation is estimated according to equation (3). Before passing to presentation of the p–δ relationship, we have to consider some other collapse modes, particularly those relating to plates without restrained edges. If reinforced concrete plates are allowed to slide over the supports, then at a certain magnitude of deflection there appears in rectangular plates a crack perpendicular to the longer side of the plate. This crack passes across the thickness of the plate, but no rotation of the adjacent parts of the slab with respect to the crack is observed. The first one who noticed that fact seems to be Wood, [2]. Experiments by Jaeger, [8], also provide valuable data in this respect. The above-mentioned collapse mode is shown in Fig. 4. The motion of the collapse mechanism in comparison to that shown in Fig. 3 involves an additional rotation of the element ACDE with respect to an axis perpendicular to the plate surface. The plate element ACDE is at point D in contact with the adjacent part at the distance $\xi_0 H$ from the middle surface.

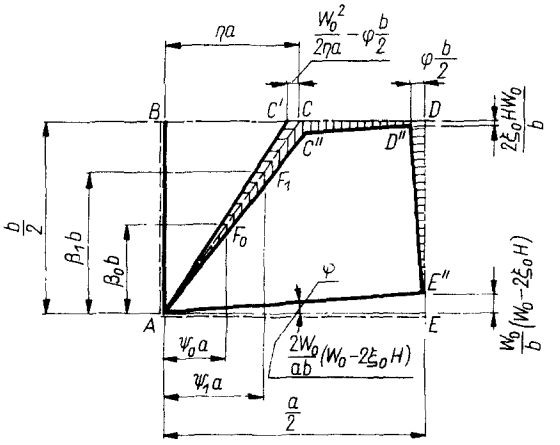

FIG. 4

Evaluation of dissipation associated with the interaction curve (15) is, for the collapse mechanism considered, somewhat cumbersome. If the following approximate assumptions are made, namely that

$$\left.\begin{aligned} M &= M_0, \quad N = 0 \quad \text{along the line } AF_1 \\ M &= 0, \quad N = N_0 \quad \text{along the line } F_1CDE \end{aligned}\right\} \tag{28}$$

the dissipation takes on the form

$$\begin{aligned} D &= M_0(\psi_1 a\dot{\theta}_{AE}+\beta_1 b\dot{\theta}_{AB})+\sum_{i=1}^{n} N_0\dot{\Lambda}_i l_i + N_0 H\left(\frac{a}{2}\dot{\theta}_{AE}+\frac{b}{2}\dot{\theta}_{BA}-\psi_1 a\dot{\theta}_{AE}-\beta_1 b\dot{\theta}_{BA}\right) \\ &= M_0 W_0\beta_1\frac{4\eta^2\alpha^2+1}{\eta\alpha}+N_0 W_0^2\frac{2\eta\alpha^2-4\eta^2\alpha^2+1}{4\eta\alpha} \\ &\quad + N_0 W_0 H\left(\xi_0\frac{\alpha}{2}+\frac{2\eta\alpha^2+1}{2\eta\alpha}-\xi_0\beta_1\frac{4\eta^2\alpha^2+1}{2\eta\alpha}\right). \end{aligned} \tag{29}$$

For the considered collapse mode as shown in Fig. 4 extension of the bending response is

$$\beta = \frac{\xi_0}{2\delta_0(1-2\eta)+4\eta\xi_0}, \qquad \psi = 2\eta\beta. \tag{30}$$

whereas the dissipation (29) is computed according to (28), assuming that the segments AECD are in contact at the distance H from the middle surface. Thus

$$\beta_1 = \frac{1}{2\delta_0(1-2\eta)+4\eta\xi_0}, \qquad \psi_1 = 2\eta\beta_1. \tag{31}$$

It is seen that the bending zone extent depends upon the deflection magnitude δ_0 and on the position of contact of the AECD-parts at the plate center.

In the evaluation of the dissipation function (29) it has been tacitly assumed that the compressive forces are transmitted by the plate without any energy dissipation.

Another collapse mode involving tension cracks is also possible. It is shown in Fig. 5. In this case the bending moments are acting along the hinge ACD, whereas the axial extension is concentrated on the line FC. The associated dissipation consists of the bending dissipation as given by (26) whereas, when including the additional term due to stretching, we have

$$D = M_0 \dot{W}_0 \left[\alpha + \frac{1}{2\eta\alpha} + \delta_0 \frac{1}{\eta\alpha(3+\xi_0)}\right]. \tag{32}$$

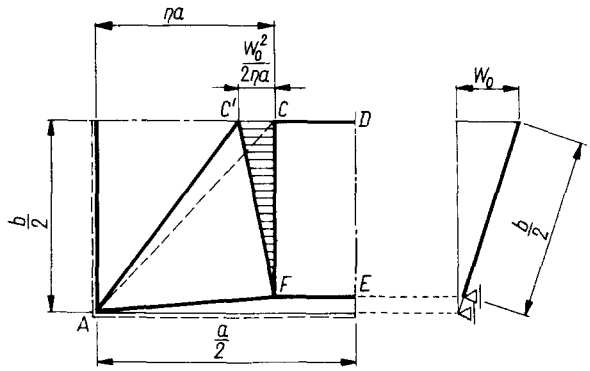

FIG. 5

Having derived expressions for the dissipation function, we can proceed to the evaluation of the load–deflection relations.

5. LOAD–DEFLECTION RELATIONSHIP

The load–deflection relation beyond the plastic collapse in dimensionless form can be written as follows

$$\lambda = \frac{p}{p_0} = \frac{D}{D_0}, \tag{33}$$

where p denotes the actual load, p_0 being the bending collapse load.

For a plate with restrained boundaries, substitution of (26) and (27) into (33), after certain rearrangements, yields the results

$$\lambda = 1 \qquad \delta \leq \xi_0 \tag{34}$$

$$\lambda = C - D(1+B)\delta_0 + E(1+2B)\delta_0^2 - CA\frac{\xi_0^2}{6\delta_0}, \qquad \xi_0 \leq \delta_0 \leq 1, \tag{35}$$

$$\lambda = G + G(1+B)\delta_0 - AGF\frac{1}{\delta_0}, \qquad \delta_0 \geq 1. \tag{36}$$

The values of coefficients A, B, C, D, E, and F are contained in Tables 1 and 2.

TABLE 1

α	1·0	1·2	1·4	1·6	1·8	2·0
$A = \dfrac{1+4\eta^2\alpha^2}{1+2\eta\alpha^2}$	1·000	0·947	0·897	0·843	0·794	0·750
$B = \dfrac{2\eta\alpha^2-4\eta^2\alpha^2}{1+2\eta\alpha^2}$	0·000	0·054	0·104	0·158	0·206	0·250

TABLE 2

ξ_0	0·0	0·6	0·7	0·8	0·9	1·0
$C = \dfrac{3-\xi_0}{(3+\xi_0)(1-\xi_0)}$	1·000	1·667	2·070	2·875	5·380	∞
$D = \dfrac{1+5\xi_0}{2(3+\xi_0)(1-\xi_0)}$	0·167	1·398	2·030	3·290	7·050	∞
$E = \dfrac{4}{3(3+\xi_0)(1-\xi_0)}$	0·444	0·926	1·200	1·750	3·420	∞
$F = \dfrac{1-2\xi_0+\xi_0^2}{12}$	0·0833	0·0133	0·0075	0·0033	0·0008	0
$G = \dfrac{2}{3+\xi_0}$	0·667	0·555	0·540	0·527	0·513	0·500

For the collapse mode shown in Fig. 4 substitution of (29) into (33) yields for the range $\delta_0 \geq \xi_0$ the following result:

$$\lambda = GI\delta_0 + G(1+\xi_0 K) + \beta_1 A[2-G(2+\xi_0)], \qquad \xi_0 \leq \delta_0. \tag{37}$$

From relations (26), (32) and (33) the load–deflection relationship associated with the collapse mode shown in Fig. 5 is found to be linear in terms of δ_0, namely

$$\lambda = 1 + \left(\frac{2}{3+\xi_0}\right)\left(\frac{1}{1+2\eta\alpha^2}\right)\delta_0 = 1 + GP\delta_0. \tag{38}$$

The coefficients A and G entering equation (37) are contained in Tables 1 and 2, whereas the values of I, K and P are given in Table 3. Values of β_1 entering (37) are to be computed from (31).

TABLE 3

α	1·0	1·2	1·4	1·6	1·8	2·0
$I = 1-\dfrac{4\eta^2\alpha^2}{1+2\eta\alpha^2}$	0·500	0·486	0·485	0·496	0·502	0·527
$K = \dfrac{2\eta\alpha^2}{1+2\eta\alpha^2}$	0·500	0·567	0·604	0·661	0·694	0·723
$P = \dfrac{1}{1+2\eta\alpha^2}$	0·500	0·433	0·396	0·339	0·306	0·277

For the sake of comparison in Fig. 6 there are presented the load–deflection relationships for the case of $\alpha = 2$. Fig. 6(a) concerns $\xi_0 = 0{\cdot}6$, thus it corresponds to the reinforcement percentage $\mu = 1\,\%$, whereas in Fig. 6(b) the diagrams are shown as corresponding to $\xi_0 = 0$.

It can be seen that the collapse mode shown in Fig. 3 can give smaller values of the limit load only for deflection of the order of magnitude of the plate thickness. With increasing deflections the collapse modes with one or two transverse cracks are associated with a lower value of the load. Fig. 6(b) shows that a situation may arise when the collapse mode of type shown in Fig. 4 is more probable than that of Fig. 5. It is also seen that

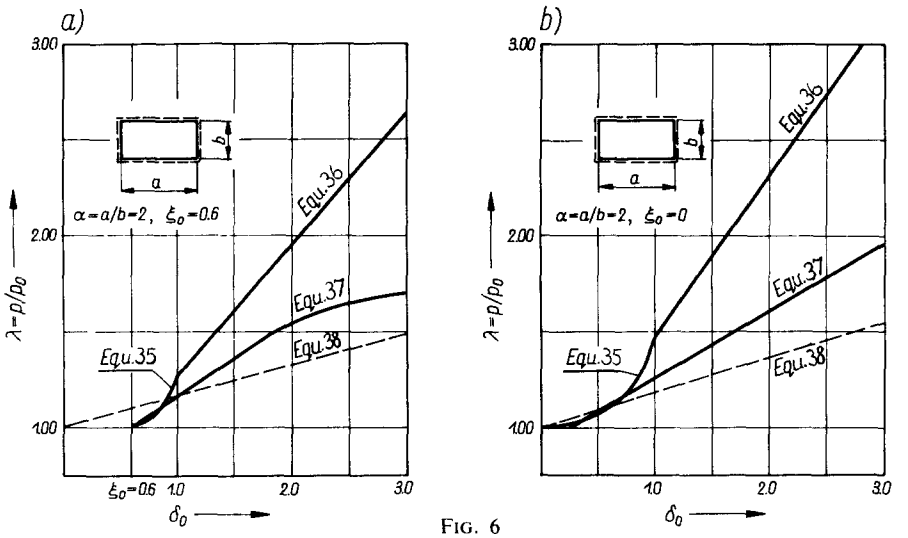

FIG. 6

plates with boundaries allowed to slide show smaller increase of load as the deflections are increasing.

Our concern now will be a comparison between the approximate load–deflection relationships obtained for rectangular plates, and experimental data.

6. DESCRIPTION OF MODELS AND TEST ARRANGEMENTS

Tests were made on plates $2{\cdot}0\,\text{m} \times 1{\cdot}0\,\text{m}$, $a/b = 2$ and $1{\cdot}6\,\text{m} \times 1{\cdot}1\,\text{m}$, $a/b = 1{\cdot}45$. The plate thickness was $3{\cdot}0\,\text{cm}$, the effective thickness $2H = 2{\cdot}6\,\text{cm}$. The models were made of concrete of average compressive strength $R_c = 175\,\text{kg/cm}^2$, measured on cylinders ϕ 16 cm, $l = 16\,\text{cm}$. The models were reinforced with mild steel mesh made of annealed ϕ 3 mm wires. Two types of isotropic mesh were used, namely reinforcement type I, ϕ 3 at 3 cm spacing, reinforcement percentage $\mu = 0{\cdot}907\,\%$, and type II, ϕ 3 at 6 cm spacing, reinforcement percentage $\mu = 0{\cdot}453\,\%$. The yield point stress of wires was $\sigma_0 = 2690\,\text{kg/cm}^2$, the tensile strength $R_0 = 3540\,\text{kg/cm}^2$. In computing the theoretical collapse load the tensile strength R_0 has been substituted into the yield moment formula.

According to (12) the ultimate yield forces and the ultimate moment are, respectively,

$$N_0 = F_z R_0 = \begin{cases} 8350\ \text{kg/m, type I,} & (39) \\ 4175\ \text{kg/m, type II,} & (40) \end{cases}$$

$$M_0 = F_z R_0 \left(2H - \frac{F_x R_0}{2R_c}\right) = \begin{cases} 192{\cdot}5\ \text{kgcm/cm, type I,} & (41) \\ 102{\cdot}4\ \text{kgcm/cm, type II.} & (42) \end{cases}$$

The theoretical values of the bending collapse load, computed according to the relation, (cf. [14])

$$p_0 = 6M_0/a^2\eta^2 \tag{43}$$

are given in Table 4.

TABLE 4

α	1·45		2·00	
η	0·405		0·326	
Reinforcement	Type I	Type II	Type I	Type II
$\mu\,\%$	0·907	0·453	0·907	0·453
σ_0 | p_0(kg/m²)	2145	1135	2110	1120
R_0 | p_0(kg/m²)	2750	1465	2720	1445

In order to eliminate the influence of tensioned concrete on the yield moment and on the bending collapse load the tensioned zone of concrete along the theoretical hinge lines has been disrupted by an arrangement of flat bars with reduced bond between the steel and concrete.

Models were placed on a test bed consisting of a steel box without a deck. Water pressure was applied to the bottom face of a test slab. Along the edges the slab contacted an appropriate arrangement of supporting hinges, allowing for rotation and sliding of the plate over the supports.

Loading was performed with a constant velocity. The constancy of loading velocity was assured by an electronic control device. Deflections of the plate center as well as rotations at two points on the yield hinge were measured by means of mechanical devices. The increase of loading, deflections and rotations were recorded automatically on a paper tape.

Two identically reinforced models were tested for each plate size and reinforcement amount.

7. TEST RESULTS

In Figs. 7, 8 and 9 the results of deflection measurements are presented in the form of load–deflection relationships for a plate center. The solid lines denote the experimentally obtained relations between the applied pressure and the dimensionless deflection $\delta_0 = W_0/2H$. The plates were loaded up to deflections of magnitude $W \simeq 20$ cm, thus $\delta_0 \simeq 7{\cdot}5$.

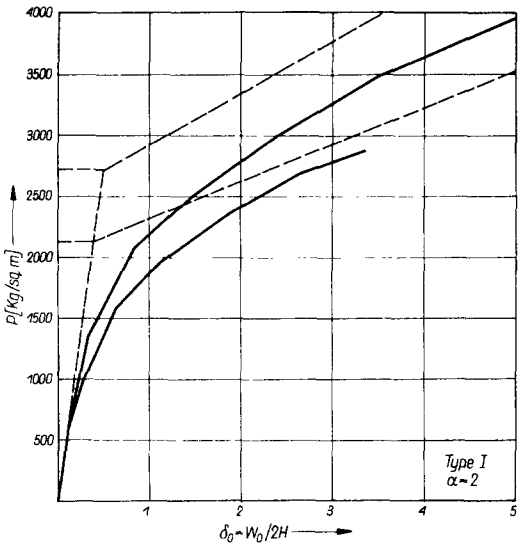

FIG. 7

Since the results of measurements represent the total deflection i.e. the elastic and the irreversible one, it is necessary to take this fact into account when comparing the obtained load–deflection relationships with those following from formulas derived in Section 5 for rigid-plastic plates. Although it is not fully justified, elastic deflections have been added to those of post-yield response. The resulting curves are shown in Figs. 7–9 by broken lines. When computing the elastic deflections it has been assumed that up to the collapse load p_0 the plates respond linearly elastic and for $p > p_0$ their response is purely plastic. Two values of p_0 are indicated in the figures. The lower one corresponds to the steel yield stress σ_0, the upper one to the ultimate strength R_0, (cf. Table 4). Obviously the upper theoretical curve should run above that obtained from experiments.

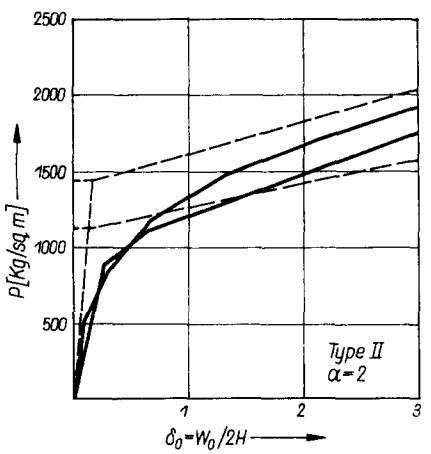

FIG. 8

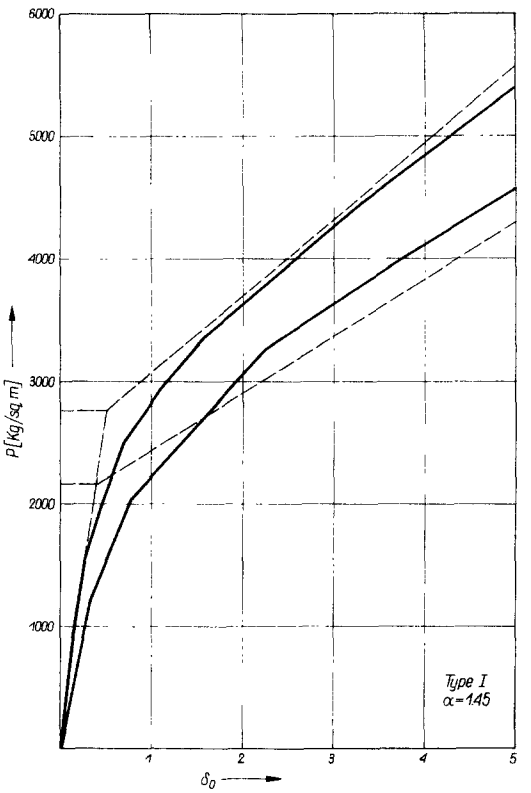

FIG. 9

As it was clearly seen from Fig. 6, the lowest theoretical load–deflection relation for plates with unrestrained boundary is that associated with the collapse mode shown in Fig. 5. Thus the experimental results have been compared with those following from the formula (38).

Elastic deflections at the plate center were computed according to the relation (cf. [15])

$$W = \beta p a^4/D, p \leq p_0 \tag{44}$$

where $\beta = 0{\cdot}00739$ for $b/a = 1{\cdot}45$ and $\beta = 0{\cdot}01013$ for $b/a = 2{\cdot}0$. The bending rigidity was taken $D = EI$ and the inertia moment I has been substituted for a fissurated plate. For $R_c = 175\,\text{kg/cm}^2$, $\sigma_0 = 2690\,\text{kg/cm}^2$, $n = \sigma_0/R_c = 15$ and Young's modulus $E = 160000\,\text{kg/cm}^2$ the rigidities were found to be $D = 2{\cdot}18 \times 10^7\,\text{kgcm}^2/\text{m}$ for $\mu = 0{\cdot}907\,\%$ and $D = 1{\cdot}44 \times 10^7\,\text{kgcm}^2/\text{m}$ for $\mu = 0{\cdot}453\,\%$.

In Figs. 10 and 11 the obtained collapse modes are shown for two cases of plate size. The tensile cracks perpendicular to the longer edge are clearly visible. Position of these cracks is that as idealized in Fig. 5.

Fig. 12 is presented in order to give an idea of the magnitude of permanent deformation of tested plates.

The experimental data as demonstrated in Figs. 7–12 are in agreement with the theoretical results of the developed method of post-yield analysis for reinforced concrete

FIG. 10. Collapse mode for plates $a/b = 2{\cdot}0$.

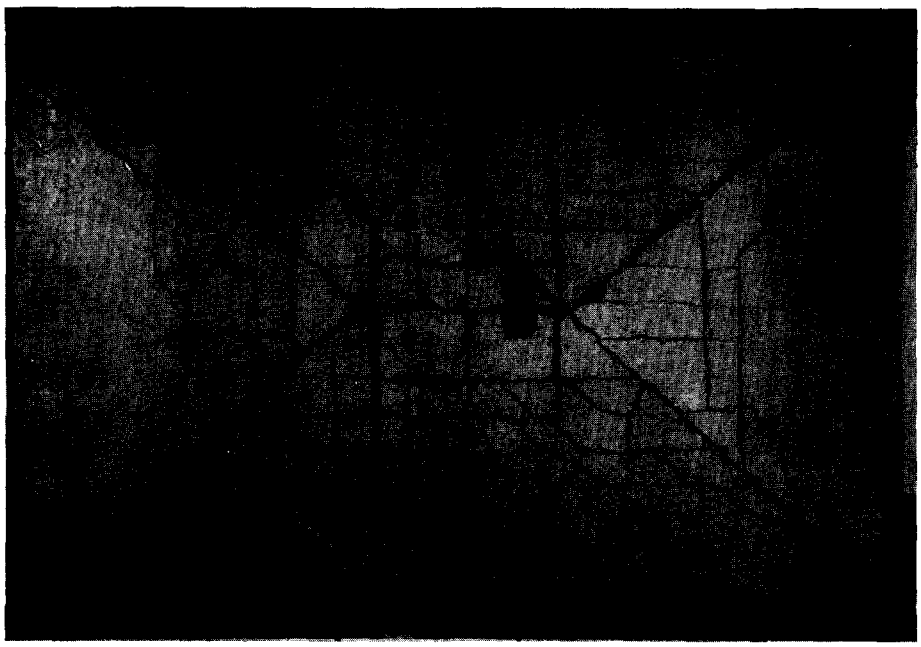

FIG. 11. Collapse mode for plates $a/b = 1{\cdot}45$.

[*facing page 110*

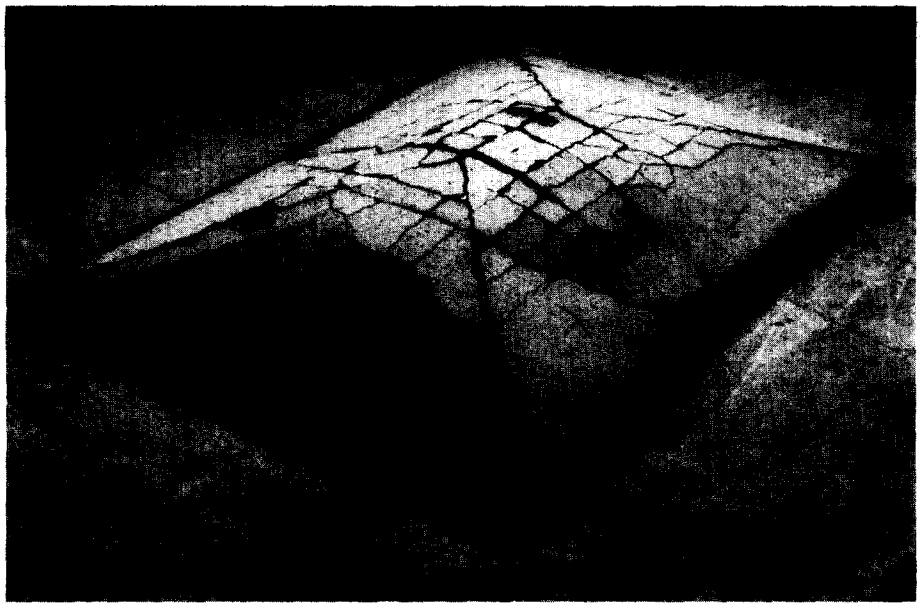

FIG. 12. Permanent deflection due to membrane action in bending.

plates. It is seen that the influence of geometry changes on the carrying capacities of plates can be significant, especially for plates with restrained edges. Since such cases generally occur in structures, the large-deflection theory of reinforced concrete plates seems to be worth pursuing in application to orthotropic plates as well as for other boundary conditions.

Acknowledgment—The authors are indebted to Professor A. Borcz and Mr. J. Sieczkowski from the Polytechnic Institute of Wroclaw for very carefully performed experiments. The photographs presented in the paper were made by Mr. E. Witecki.

REFERENCES

[1] A. A. GVOZDEV, *Stroit. Prom.* **17**, No. 3, 51 (1939).
[2] R. H. WOOD, *Plastic and Elastic Design of Slabs and Plates*, Thames and Hudson, London (1961).
[3] E. T. ONAT and R. T. HAYTHORNTHWAITE, *J. appl. Mech.* **23**, 49 (1956).
[4] Ü. LEPIK, *Izv. AN SSSR, Mekh. i Mash.* No. 2, 78 (1960).
[5] P. G. HODGE, *Limit of Analysis of Rotationally Symmetric Plates and Shells*, Prentice Hall, Englewood Cliffs, N.J. (1963).
[6] A. R. RZHANITZYN, *IX^e Congr. Int. Mec. Appl. (Bruxelles, 1956) Act.* **6**, 331 (1956).
[7] A. SAWCZUK, *J. Méc.* **3**, 15 (1964).
[8] TH. JAEGER, *Beton u. Stahlbetonb.* **37**, 262 (1962).
[9] A. SAWCZUK, M. JANAS and J. ZAWIDZKI, *Rozpr. Inz.* **10**, 243 (1962).
[10] A. SAWCZUK and L. WINNICKI, *Arch. Inz. Lad.* **9**, 461 (1963).
[11] Z. MRÓZ, *Arch. Mech. Stos.* **12**, 85 (1960).
[12] A. SAWCZUK and W. OLSZAK, *Proceedings of Simplified Calculation Methods (Brussels, 1961)* North Holland, Amsterdam (1962).
[13] K. W. JOHANSEN, *Yield-line Theory*, Cement and Concrete Association, London (1962).
[14] A. SAWCZUK and TH. JAEGER, *Grenztragfähigkeits-Theorie der Platten*, Springer, Berlin (1963).
[15] S. P. TIMOSHENKO and S. WOINOWSKY-KREIGER, *Theory of Plates and Shells*, McGraw-Hill, New York (1959).

(*Received* 30 *May* 1964)

Résumé—L'expérience a démontré que le pouvoir portant des dalles est supérieur à celui qui résulterait de la théorie des lignes de rupture. Le comportement des constructions plastiques au-delà de la charge limite de flexion subit l'influence des changements de la géométrie d'une structure au cours de sa déformation plastique. L'article présente une étude du rapport charge/flèche pour dalles rectangulaires en béton armé à appui simple. On constate que l'"effet de membrane" se trouve localisé dans les zones des rotules plastiques de flexion. En conséquence, les zones d'effet de membrane s'accroissent à mesure que la charge augmente. Une méthode cinématique d'analyse des dalles plastiques au-delà de la charge limite en flexion est présentée; des modes de rupture cinématiquement admissibles sont étudiés et les fonctions de dissipation qui les accompagnent en sont dérivées. Des rapports charge/flèche sont obtenus pour différents mécanismes de rupture. Les résultats théoriques sont comparés avec les données expérimentales obtenues par essais sur modèles.

Абстракт—Из опытов известно, что действительная грузо-несущая способность плиты является большей, чем предсказанная по теории предельной нагрузки. Поведение пластических структур за пределом изгибающей критической нагрузки зависит от изменения геометрии структуры во время процесса пластической деформации. В настоящей работе рассматриваются отношения между нагрузкой и прогибом в прямоугольных железо-бетонных плитах, имеющих простую опору. Найдено, что действие растяжимой мембраны локализовано в зонах поддающихся перегибу пунктов. С увеличением нагрузки образуются зоны чистых мембранных реакций. Работа предлагает кинематический метод анализа пластических плит за пределом критической сгибающей нагрузки. Рассматриваются кинематически допустимые случаи разрушения и выводятся ассоциированные диссипативные функции. Получены отношения нагрузки к прогибу для различных схем смещений. Теоритические результаты сравниваются с экспериментальными данными, полученными из испытаний на модели.